Journal of Computational Physics 228 (2009) 4745–4756

Contents lists available at ScienceDirect

Journal of Computational Physics

journal homepage: www.elsevier.com/locate/jcp

Efficient solution of the Schroedinger–Poisson equations in layered semiconductor devices

Christopher R. Anderson *

Department of Mathematics, University of California, Los Angeles, Box 951555, Los Angeles, CA 90095-1555, United States

ARTICLE INFO

Article history:
Received 21 July 2008
Received in revised form 19 March 2009
Accepted 21 March 2009
Available online 7 April 2009

Keywords:
Schroedinger–Poisson
Quantum dots
Electronic structure
Computational nano-technology

ABSTRACT

In this paper we present several mathematical models that can be used to create approximate solutions of the three-dimensional Schroedinger–Poisson equation in layered semiconductor devices. A general algorithmic strategy that can be used to create efficient solution procedures for each of these models is described. Computational results demonstrating the accuracy and efficiency that can be obtained with the use of these models is presented.

1. Introduction

Recent interest in quantum information processing has led to a focus on the design of layered semiconductor devices that allow one to directly control electron confinement and to manipulate isolated electronic states (quantum dots) through electrostatic and magnetic fields. (For an excellent overview of the physics of few-electron quantum dots, see [8].) In such devices, vertical confinement of electrons is accomplished by a combination of an applied potential and quantum wells created by the layering of materials with differing band offsets. Lateral confinement of the electrons is accomplished by an applied potential whose form is determined by the gate structure on the surface of the device and voltages applied to these gates. The structure of one of these devices is shown in Fig. 1. The need for simulation arises because of the necessity to explore a large number of device structure and gate configuration parameters to find those designs that are likely to lead to functional devices. In this paper we present several mathematical models that can be used to create a family of approximate solutions to the three-dimensional Schroedinger–Poisson equations used to simulate layered semiconductor devices. We also present a general algorithmic strategy for solving the equations of these models and demonstrate through computational results that it is possible to create highly efficient simulations of three-dimensional layered semiconductor devices.

In the preliminary design of layered semiconductor devices for quantum computing, one is principally interested in developing devices in which the electronic structure can be controlled by an appropriate application of gate voltages. For this task, the Schroedinger–Poisson model, a model where the electrostatic interactions of the electrons are included but spin effects are ignored, is used directly [4–6,10,11,20,21] or as part of a multi-scale approach [14,15,25]. The benefit of using a Schroedinger–Poisson model is that the states in the model are obtained by solving a one particle Schroedinger operator rather than a multi-particle Schroedinger operator. Even with the simplifications afforded through the use of this model, the computational task can be quite demanding, especially when one is required to run hundreds, if not thousands, of

* Tel.: +1 310 825 1298; fax: +1 310 206 2679.
E-mail address: anderson@math.ucla.edu

0021-9991/$ - see front matter © 2009 Elsevier Inc. All rights reserved.
doi:10.1016/j.jcp.2009.03.037

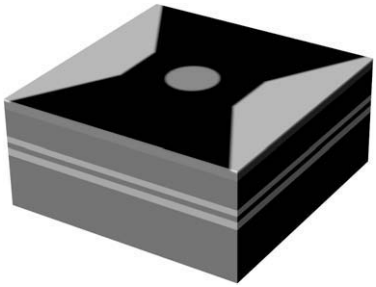

Fig. 1. Sample device geometry. Lightly shaded regions on top indicate the location of the applied potential (gates). Lightly shaded regions internally indicate InGaAs layers.

simulations to explore parameter space during a design process. To reduce the computational cost of such explorations, one often employs simplified models, models whose solutions can be computed much more efficiently than the solutions to the complete Schroedinger–Poisson model.

The one-dimensional and two-dimensional Schroedinger–Poisson models are commonly used approximate models [9,13,19], and in this paper we present other approximate models that can be used, in particular models that are especially appropriate for simulating three-dimensional devices with non-separable geometry. These additional models arise from asking the mathematical question "what simplified mathematical structure would allow us to create solutions more efficiently" rather than by asking "what simplified physics would allow us to create solutions more efficiently". Since these models originate with a desire to compute fast solutions, and not adhere to any particular physics principles, there is some question as to their utility. We are pleased to report, and will demonstrate through computational results, that the simplified models presented work very well and provide answers of sufficient accuracy for many design questions. Moreover, with the use of these models, the computation time is often reduced by one to two orders of magnitude.

With the existence of several models, one or more of which may be used in any specific design investigation, comes the problem of creating implementations for each of them. In this paper we describe a general algorithmic strategy that can be used for all of the models presented. The main feature of this algorithmic strategy consists of transforming the problem of solving the equations "self-consistently" into one of evolving a time-dependent partial differential equation to steady-state using a family of stabilized Runge–Kutta methods [2]. This latter procedure can be implemented as a "generic" code, and, through the use of object oriented computing techniques, is applied to each of the models described. In this approach, computational efficiency is obtained by creating efficient implementations of methods for solving Poisson's equation and Schroedinger's equation. We will describe how efficient solution procedures for each of these equations that can be obtained by exploiting the layered structure of the devices. One aspect of the algorithmic strategy described is that it does not require the formation of gradients of the non-linear system of equations that must be solved. In this regard it differs from the procedures described in [10,13,11,20,21] and possesses linear convergence behavior. We have been willing to accept this linear rate of convergence in exchange for simplicity of implementation, robustness with respect to numerical parameters and alternate models, and a running time that has proven to be quite acceptable.

The algorithmic procedure and models described in this paper can easily accommodate additional physics such as surface charge accumulation models or an exchange-correlation potential correction. However, there is a wide range of additional physics, e.g. magnetic field dependence and multi-band effects that have been [4,11,14,15] and are currently incorporated [17,22] in existing Schroedinger–Poisson based device simulations. We expect that many of the ideas presented in this paper can also lead to the improvement of existing simulations or the creation of new simulations that incorporate such physics.

In the next section of this paper we present the equations for the Schroedinger–Poisson model and then give the equations associated with commonly used simplified models and additional models that have proven useful for the creation of efficient codes. In the third section we describe the general computational strategy that is used for all of the model equations and give specific details that enable efficient implementations. In the last section we present computational results.

2. Schroedinger–Poisson equations

2.1. 3D Schroedinger–Poisson equations

The Schroedinger–Poisson model is a coupled system of PDE's consisting of an equation for the potential (1) and a single particle Schroedinger equation (2).

$$\nabla \cdot (\vec{\kappa}(\vec{x}) \cdot \nabla \phi(\vec{x})) = q\rho(\vec{x}), \tag{1}$$

$$-\frac{\hbar^2}{2}\nabla \cdot (\vec{\beta}(\vec{x}) \cdot \nabla \Psi(\vec{x})) + [\phi(\vec{x}) + \Delta E_c(\vec{x})]\Psi(\vec{x}) = E\Psi(\vec{x}). \tag{2}$$

The use of these equations assumes that the electrons interact solely through the electrostatic field and spin effects are ignored.

In the equation for the potential (1), $\vec{\kappa}(\vec{x})$ is the vector of dielectric coefficients and $\rho(\vec{x})$ is the electron density. In the single-particle Schroedinger equation (2), $\Psi(\vec{x})$ is the wave function, E the energy, $\vec{\beta}(\vec{x}) = \left(\frac{1}{m_x^*(\vec{x})}, \frac{1}{m_y^*(\vec{x})}, \frac{1}{m_z^*(\vec{x})}\right)$ is the vector of effective mass coefficients, and ΔE_c the pseudopotential energy due to the band offset at the heterointerfaces. As a consequence of the layered structure of the devices being considered, the vector of dielectric coefficients $\vec{\kappa}(\vec{x})$, the effective mass coefficients, $\vec{\beta}(\vec{x})$, and the pseudopotential energy, ΔE_c, are piecewise constant functions in the vertical direction. The electron density $\rho(\vec{x})$ is given by

$$\rho(\vec{x}) = -N_D(\vec{x}) + \sigma_b(\vec{x}) - n(\vec{x}). \tag{3}$$

Here, $N_D(\vec{x})$ is the ionized doping density, $\sigma_b(\vec{x})$ a background hole concentration, and $n(\vec{x})$ is the density of bound state electrons. In the zero-temperature limit the bound state electron density takes the form

$$n(\vec{x}) = 2\sum_{E_k<E_F} \Psi_k^*(\vec{x})\Psi_k(\vec{x}), \tag{4}$$

where, as indicated, the sum is over the states whose energy E_k is less than the Fermi energy E_F. The factor of 2 accounts for the spin degeneracy.

When solving (1) for $\phi(\vec{x})$, periodic boundary conditions are assumed for the transverse directions and homogeneous Dirichlet conditions are used at the top and bottom boundaries of the computational domain (a slight modification of the procedure allows one to accommodate alternate boundary conditions, e.g. surface charge boundary conditions). At the bottom boundary ($z = L$) of the computational domain the potential $\phi(\vec{x})$ is set to a value ϕ_∞, where ϕ_∞ is given by

$$\phi_\infty = \left(\frac{3\pi^2\hbar^3\sigma_s}{2\sqrt{2}m^{3/2}}\right)^{\frac{2}{3}} + E_f. \tag{5}$$

This formula is derived by requiring that the induced charge in a uniform substrate cancels a background hole concentration, σ_s, in the substrate. The depth, L, at which the boundary condition is enforced is empirically chosen to be of sufficient size so that any increase in size induces only negligible changes in the computed potential.

The boundary conditions for the wave functions determined by Schroedinger's equation, (2), consist of periodic boundary conditions in the transverse directions and homogeneous Dirichlet conditions at the top and bottom boundaries of the computational domain. Typically, the vertical extent of the computational domain used to solve (2) is taken to be much smaller than the full vertical extent of the device. This is an acceptable procedure because for layered quantum well devices the bound state wave functions are strongly localized in the vertical direction about the quantum wells.

2.2. The reduced dimension Schroedinger–Poisson equations

The Schroedinger–Poisson equations (1) and (2) consist of a coupled systems of PDE's for functions of three spatial variables. In many circumstances, the potential in a device will only have variation in the vertical direction, $\phi(x,y,z) = \phi(z)$, or only variation in the vertical direction and a single transverse direction, $\phi(x,y,z) = \phi(y,z)$. In such cases, the equations (1) and (2) can be transformed into a set of equations of reduced spatial dimension. The foundation for this reduction is the separability of the Schroedinger operator under these assumptions. When there is no transverse variation in the potential boundary conditions, the dielectric constants, the doping densities and the background hole concentrations, the potential associated with a solution of (1) will be a function of the vertical coordinate alone, e.g. $\phi(x,y,z) = \phi(z)$. If the vector of effective mass coefficients also has the form $\vec{\beta}(\vec{x}) = \tilde{\beta}(z) = \left(\frac{1}{m_x^*}, \frac{1}{m_y^*}, \frac{1}{m_z^*(z)}\right)$ then the eigenfunctions of (2) are of the form

$$\Psi(x,y,z) = \eta(z)e^{2\pi i k_x \frac{x}{D}}e^{2\pi i k_y \frac{y}{D}},$$

where D is the size of the periodic domain in the transverse directions. If one inserts these specific forms for ϕ and Ψ into the Schroedinger equations (2) and uses the technique of separation of variables one obtains (after letting $D \to \infty$) the 1D Schroedinger–Poisson equations

$$\frac{d}{dz}\left(\kappa(z)\frac{d\phi(z)}{dz}\right) = q\rho(z), \tag{6}$$

$$-\frac{\hbar^2}{2}\frac{d}{dz}\left(\beta_z(z)\frac{d\eta}{dz}\right) + [\phi(z) + \Delta E_c(z)]\eta(z) = E\eta(z) \tag{7}$$

with $\beta_z(z) = \frac{1}{m_z^*(z)}$, the electron density $\rho(z)$ given by

$$\rho(z) = -N_D(z) + \sigma_b(z) - n^{(1)}(z) \tag{8}$$

and $n^{(1)}(z)$ is defined by

$$n^{(1)}(z) = 2\sum_{E_k<E_F} D_k^{(2)}\eta_k^*(z)\eta_k(z). \tag{9}$$

Here $D_k^{(2)}$ is the 2D density of states functional

$$D_k^{(2)} = \begin{cases} \frac{(E_F-E_k)\sqrt{|m_y||m_x|}}{2\pi\hbar^2} & E_k < E_F, \\ 0 & E_k \geqslant E_F. \end{cases} \tag{10}$$

For a derivation of the 2D density of states functional, and information about how to include the effects of finite temperature, see [18].

Similarly, under those circumstances where the potential has only transverse variation in one direction, $\phi(x,y,z) = \phi(y,z)$, then the eigenfunctions of (2) are of the form

$$\Psi(x,y,z) = \eta(y,z)e^{2\pi i k_x \frac{x}{D}}.$$

If one follows a procedure similar to the derivation of the 1D Schroedinger–Poisson equations, one obtains the 2D Schroedinger Poisson equations

$$\nabla\cdot(\kappa(y,z)\nabla\phi(y,z)) = q\rho(y,z), \tag{11}$$

$$-\frac{\hbar^2}{2}\nabla\cdot(\tilde{\beta}(y,z)\cdot\nabla\eta(y,z)) + [\phi(y,z) + \Delta E_c(y,z)]\eta(y,z) = E\eta(y,z) \tag{12}$$

with $\tilde{\beta}(y,z) = \left(\frac{1}{m_y^*(y,z)}, \frac{1}{m_z^*(y,z)}\right)$, the electron density $\rho(y,z)$ given by

$$\rho(y,z) = -N_D(y,z) + \sigma_b(y,z) - n^{(2)}(y,z) \tag{13}$$

and $n^{(2)}(y,z)$ is defined by

$$n^{(2)}(y,z) = 2\sum_{E_k<E_F} D_k^{(1)}\eta_k^*(y,z)\eta_k(y,z). \tag{14}$$

Here $D_k^{(1)}$ is the 1D density of states functional [18].

$$D_k^{(1)} = \begin{cases} -\frac{\sqrt{2(E_F-E_k)}\sqrt{|m_x|}}{\pi\hbar} & E_k < E_F, \\ 0 & E_k \geqslant E_F. \end{cases} \tag{15}$$

In a typical layered device all coefficients of the effective mass will vary with the vertical coordinate, e.g. $\vec{\beta}(\vec{x}) = \left(\frac{1}{m_x^*(z)}, \frac{1}{m_y^*(z)}, \frac{1}{m_z^*(z)}\right)$. In such cases the separability assumption underlying the above derivation is not satisfied. However, quite reasonable approximate models can be obtained by approximating $m_y^*(z)$ and $m_x^*(z)$ by their values in the layers forming the quantum wells. When such approximations are made, we refer to Eqs. (6)–(10) as the 1D Schroedinger–Poisson equations and (11)–(15) as the 2D Schroedinger–Poisson equations.

2.3. 2D and 3D separable approximations

The most computationally demanding aspect in the numerical solution of the Schroedinger–Poisson equations is the solution of the eigenproblem (2). One approach to improving the efficiency of codes for solving the Schroedinger–Poisson equations consists of approximating the problem specified by (1) and (2) by sets of equations whose eigensystem calculation is not as computationally demanding. For example, if one is modeling devices where the potential is well approximated by a function of one or two variables, then one can use the 1D or 2D Schroedinger–Poisson equations described above to reduce the computational cost. Below we describe other sets of approximate equations whose solutions can be obtained at greatly reduced computational cost. The solutions obtained with these approximations are often sufficiently accurate to be used as an alternative to those obtained by solving (1) and (2), or as solutions to provide good initial iterates and/or an eigensystem basis required for the solution of (1) and (2).

The reduced computational cost of the 1D and 2D Schroedinger–Poisson equations is primarily due to the reduced spatial dimension of the eigenproblems (7) and (12) associated with these sets of equations. The reduced dimension of the eigenproblems occurs because the form of the potential allows one to use the technique of separation of variables and a three-dimensional eigenproblem (2) is transformed into that of solving a one-dimensional and a two-dimensional eigenproblem. In the case of the 1D Schroedinger–Poisson equations, the one-dimensional eigenproblem is given by (7) and is solved numerically while the two-dimensional eigenproblem is solved analytically with results implicitly incorporated in the density of states functional (10). Similarly, in the 2D Schroedinger–Poisson equations, the two-dimension eigenproblem is given by (12) and is solved numerically, while the one-dimensional eigenproblem is solved analytically with results implicitly incorporated into the 1D density of states functional (15).

Observing that the reduction in the dimension of the eigenproblem occurs because of the separable nature of the Schroedinger operator leads one to consider sets of approximate equations where the original potential equation (1) is retained but

the potential term, ϕ, occurring in the Schroedinger equation, (2), is replaced by an approximate potential $\Phi(\vec{x})$. This latter potential is functionally dependent upon ϕ and is constructed so that first, it well approximates ϕ, and second, it has a form that leads to eigenproblems with product eigenfunctions, e.g. eigenfunctions that can be calculated by solving two lower dimensional eigenproblems.

There are several choices for $\Phi(\vec{x})$. Given a solution ϕ of (1), a particularly useful choice of $\Phi(\vec{x})$ for the 3D Schroedinger–Poisson equations in layered quantum well devices is

$$\Phi(\vec{x}) = \tilde{\phi}_1(z) + \tilde{\phi}_2(x,y), \tag{16}$$

where

$$\tilde{\phi}_1(z) = \frac{1}{L_x L_y}\int\int \phi(x,y,z)\,\mathrm{d}x\,\mathrm{d}y - \frac{1}{2}\bar{\phi}, \quad \tilde{\phi}_2(x,y) = \frac{1}{L_z}\int \phi(x,y,z)\,\mathrm{d}z - \frac{1}{2}\bar{\phi}.$$

The computational domain is assumed to be a rectangular region with sides of lengths L_x, L_y and L_z respectively and $\bar{\phi}$ is defined as

$$\bar{\phi} = \frac{1}{L_x L_y L_z}\int\int\int \phi(x,y,z)\mathrm{d}x\,\mathrm{d}y\,\mathrm{d}z.$$

This choice of approximation has the property that the integral of ϕ is preserved, and if ϕ is already in the form of a sum of functions (16), the formulas reproduce (up to a constant) those functions. Moreover, if $\phi(x,y,z)$ is discontinuous along z coordinate lines, the discontinuity is preserved by the approximation.

When the above choice for $\Phi(\vec{x})$ is inserted for ϕ in (2), the resulting equation is separable and one is lead to the "3D separable approximation" to the Schroedinger–Poisson equations;

$$\nabla\cdot(\vec{\kappa}(\vec{x})\cdot\nabla\phi(\vec{x})) = q\rho(\vec{x}), \tag{17}$$

$$-\frac{\hbar^2}{2}\frac{\mathrm{d}}{\mathrm{d}z}(\beta_z(z)\frac{\mathrm{d}\eta}{\mathrm{d}z}) + [\tilde{\phi}_1(z) + \Delta E_c(z)]\eta(z) = \lambda\eta(z), \tag{18}$$

$$-\frac{\hbar^2}{2}\left(\frac{\partial}{\partial x}\left(\beta_x\frac{\partial\gamma}{\partial x}\right) + \frac{\partial}{\partial y}\left(\beta_y\frac{\partial\gamma}{\partial y}\right)\right) + \tilde{\phi}_2(x,y)\gamma(x,y) = \mu\gamma(x,y). \tag{19}$$

The expression for the density, $\rho(\vec{x})$, is given by (3) and in the formula for the contribution to the density from the occupied states (4), the eigenfunctions and energies of the Schroedinger operator are given by $\Psi_k = \gamma_i(x,y)\eta_j(z)$ with $E_k = \mu_i + \lambda_j$.

Similarly, to obtain sets of approximate equations for the 2D Schroedinger–Poisson equations (11) (15), a useful approximation for Φ is

$$\Phi(z,y) = \tilde{\phi}_1(z) + \tilde{\phi}_2(y), \tag{20}$$

where

$$\tilde{\phi}_1(z) = \frac{1}{L_y}\int \phi(y,z)\,\mathrm{d}y - \frac{1}{2}\bar{\phi}, \quad \tilde{\phi}_2(y) = \frac{1}{L_z}\int \phi(y,z)\,\mathrm{d}z - \frac{1}{2}\bar{\phi}$$

and

$$\bar{\phi} = \frac{1}{L_y L_z}\int\int \phi(x,y,z)\mathrm{d}y\,\mathrm{d}z.$$

When the approximation (20) is used in (12), then this leads to the "2D separable approximation" to the 2D Schroedinger–Poisson equations;

$$\nabla\cdot(\kappa(y,z)\nabla\phi(y,z)) = q\rho(y,z), \tag{21}$$

$$-\frac{\hbar^2}{2}\frac{\mathrm{d}}{\mathrm{d}z}\left(\beta_z(z)\frac{\mathrm{d}\eta}{\mathrm{d}z}\right) + [\tilde{\phi}_1(z) + \Delta E_c(z)]\eta(z) = \lambda\eta(z), \tag{22}$$

$$-\frac{\hbar^2}{2}\frac{\mathrm{d}}{\mathrm{d}y}\left(\beta_y\frac{\mathrm{d}\gamma}{\mathrm{d}y}\right) + \tilde{\phi}_2(y)\gamma(y) = \mu\gamma(y). \tag{23}$$

The expression for the density, $\rho(\vec{x})$, is given by (13) and in the formula for the contribution to the density by the occupied states (14), eigenfunctions and energies of (12) are given by $\Psi_k = \gamma_i(y)\eta_j(z)$ with $E_k = \mu_i + \lambda_j$.

2.4. Local density of states approximations

Other approximations to the Schroedinger–Poisson equations are based upon constructing approximate charge densities that do not require the numerical solution of the Schroedinger operator or only require the solution of one of the Schroeding-

er operators in the separable approximations described above. The simplest of these is the "3D local density of states approximation". The equations for this approximation consist of the original potential equation

$$\nabla \cdot (\kappa(y,z)\nabla\phi(y,z)) = q\rho(y,z) \tag{24}$$

and a contribution to the charge density from the occupied states, $n(\vec{x})$, given by

$$n(\vec{x}) = \begin{cases} -\frac{2\sqrt{2}}{3}\frac{(E_f-\phi(\vec{x}))^{\frac{3}{2}}\sqrt{m_x m_y m_z}}{\pi^2\hbar^3} & \phi(\vec{x}) < E_f, \\ 0 & \phi(\vec{x}) \geqslant E_f. \end{cases} \tag{25}$$

The assumption made here is that at a given point $\vec{x}$, the local charge density due to the occupied states is approximated by the density in a uniform material with a constant potential whose value is given by $\phi(\vec{x})$. In this approximation, no eigensystem solution is required.

A "1D quantum 2D local density of states approximation" can be obtained by using a local density of states only in the transverse directions. Specifically, a 3D separable approximation (17)–(19) is used, but the contribution to the charge density from the solutions of (19) is replaced by a local two-dimensional density of states approximation. Thus, the equations in this approximation are

$$\nabla \cdot (\kappa(y,z)\nabla\phi(y,z)) = q\rho(y,z), \tag{26}$$

$$-\frac{\hbar^2}{2}\frac{\mathrm{d}}{\mathrm{d}z}\left(\beta_z(z)\frac{\mathrm{d}\eta}{\mathrm{d}z}\right) + [\tilde{\phi}_1(z) + \Delta E_c(z)]\eta(z) = \lambda\eta(z), \tag{27}$$

where $\tilde{\phi}_1$ is constructed from ϕ using (16) and

$$\rho(\vec{x}) = -N_D(\vec{x}) + \sigma_b(\vec{x}) - n(\vec{x}), \tag{28}$$

$$n(z) = 2\sum_{E_k<E_F} D_k^{(*)}\eta_k^*(z)\eta_k(z). \tag{29}$$

Here $D_k^{(*)}$ is the 2D local density of states functional

$$D_k^{(*)} = \begin{cases} \frac{(E_F-\lambda_k-\tilde{\phi}_2(y,z))\sqrt{|m_y||m_x|}}{2\pi\hbar^2} & \lambda_k + \tilde{\phi}_2(y,z) < E_F, \\ 0 & \lambda_k + \tilde{\phi}_2(y,z) \geqslant E_F. \end{cases} \tag{30}$$

The use of these equations requires only the solution of the one dimensional eigenproblem in the vertical direction.

3. Computational solution procedure

3.1. Self-consistent iteration

The Schroedinger–Poisson equations (1) and (2) and every set of approximate equations given in the previous section have the general structure

$$\begin{aligned} L\phi &= S(\Psi), \\ H(\phi)\Psi &= E\Psi, \end{aligned} \tag{31}$$

where L is a Poisson operator, $S(\Psi)$, is the source density due to any doping and the occupied states, and $H(\phi)$ is the Schroedinger operator with a potential depending on upon ϕ. Since the source density can be evaluated for any ϕ, we can express these two equations as a single non-linear equation for the potential,

$$L\phi = S(\Psi(\phi)). \tag{32}$$

Here $S(\Psi(\phi))$ represents the functional that is evaluated by obtaining a solution to Schroedinger equations (or an approximation to it) with a given ϕ, and then constructing a source density based upon that solution.

Our solution procedure consists of first transforming this problem into a root finding problem by applying L^{-1} to both sides of (32) and rearranging terms,

$$0 = L^{-1}S(\Psi(\phi)) - \phi.$$

The solution of this equation is then found by evolving the PDE

$$\frac{\partial\phi}{\partial t} = L^{-1}S(\Psi(\phi)) - \phi \tag{33}$$

to steady-state using a "method of lines" approach and specially designed explicit Stabilized Runge–Kutta methods [2] to compute the solution of the resulting ODE's. Since the ODE methods are explicit they lead to an explicit self-consistent iteration strategy for solving equations that have the general form (31).

The reduction of the problem to one of finding a solution to a single non-linear partial differential equation is similar to the approach used in [10] and [12] where the Schroedinger–Poisson equations are transformed into a fixed point problem for the charge density. The potential was used in this work as the iteration variable because the iterative procedure converged rapidly and it allowed for easier implementation of additional charge accumulation models (e.g. internal and surface charge accumulation models).

The motivation for the use of an ODE time-stepping scheme to evolve to a solution of the self-consistent equations arises from the recognition that the "simple" self-consistent iteration with relaxation factor α for (32) has the form

$$L\phi^* = S(\Psi(\phi^n)),$$
$$\phi^{n+1} = \alpha\phi^* + (1-\alpha)\phi^n$$

and can be expressed as

$$\frac{\phi^{n+1} - \phi^n}{\alpha} = L^{-1}S(\Psi(\phi^n)) - \phi^n.$$

Thus, this commonly used iteration is equivalent to using forward Euler time-stepping to advance (33) to steady-state.

The equivalence between simple iteration with a relaxation parameter and the solution of (33) using Euler's method allows one a means of determining exactly when it is useful to use a stabilized Runge–Kutta method to improve the convergence properties of the self-consistent iteration. Specifically, if it is observed that simple iteration requires a small relaxation factor for convergence, this is equivalent to the necessity of using a small Euler timestep to obtain a solution to (33), and thus indicates that (33) is a moderately stiff system of ODE's. In such cases a p-step stabilized Runge–Kutta method should improve performance by approximately a factor of p. This follows because the interval of absolute stability scales as p^2 for the stabilized Runge–Kutta methods but requires only p function evaluations. For large p, factors other than function evaluation impact computational performance of the stabilized Runge–Kutta methods, and this effectively limits the size of p that one should use. We have found best results using $p \leqslant 10$.

There are several benefits in using an iteration strategy based upon explicit ODE time-stepping methods. The first is that the resulting iteration is gradient free, and one avoids the complications that are introduced by forming gradients of functionals that are non-linearly dependent upon an eigensystem computation. Moreover, we have found that the iteration scheme is remarkably robust and has proven a reliable method that allows for the inclusion of additional models of charge accumulation and a variety of boundary conditions. Another benefit is that the iteration strategy is independent of the dimension or any particular model of the Schroedinger operator used, a fact that can be exploited when constructing codes that implement this strategy. Specifically, one can create a single templated class that implements the stabilized Runge–Kutta methods in [2], and by using instantiations of this class, obtain an iteration procedure for all of the sets of equations described in this paper

When using iterative methods based upon explicit time-stepping techniques, computational efficiency is obtained by developing efficient procedures for the evaluation of the right hand side of (33), e.g. the functional

$$L^{-1}S(\Psi(\phi^k)) - \phi^k,$$

where ϕ^k is the potential at a particular timestep or an intermediate stage in the Runge–Kutta method. The evaluation of this functional is performed in three steps. The first step is the solution of the Schroedinger equation (or approximation to it) and the construction of the charge density based on this solution, $S(\Psi(\phi^k))$. The second step consists of determining the potential induced by this charge density, $\phi^* = L^{-1}\ S(\Psi(\phi^k))$, by solving the Poisson problem $L\phi^* = S(\Psi(\phi^k))$. The last step consists of computing $\phi^* - \phi^k$. Thus, computational efficiency of each iteration depends entirely on the construction of efficient techniques for the solution of Schroedinger's equation and Poisson's equation. In the case of layered quantum well devices, one can create discretizations and efficient solution techniques for these discretizations that exploit the specific nature of the geometry.

3.2. Computational grid

The computational grid used to solve the potential and the Schroedinger equation is block structured with each grid block having a uniform rectangular mesh. All grid blocks share the same mesh widths in the transverse directions, while in the vertical direction, the grid blocks have differing mesh widths. In order to accurately resolve the wavefunctions obtained by solving Schroedinger's equation, the mesh in the vertical direction of the grid blocks in the region near the quantum wells are highly refined. The devices under consideration are layered semiconductor devices, with the layers having different material properties. The grid blocks are constructed so that any material property discontinuity in the device is coincident with a grid block boundary.

3.3. Schroedinger's equation

The approximation of the transverse derivatives occurring in the Schroedinger operators are based upon standard high order centered finite difference approximations (up to order 8). Standard finite difference approximations can be used in

the transverse directions because the effective mass coefficients are constant within each layer, and hence each grid block. In the vertical direction, a finite volume based discretization is used, one that accommodates the discontinuous nature of the effective mass coefficients in the vertical direction and the differing mesh sizes in each of the grid blocks. With the use of the finite volume approximation one obtains a non-symmetric discretization, however by appropriate diagonal scaling, one can transform the discrete equations into an eigenproblem involving a symmetric system of equations.

When a solution of the one-dimensional Schroedinger's equation is required (e.g. when one is solving (7) or (18) or (27)) then these solutions are obtained using the linpack routine DSTEVX [3]. This routine was selected because it has the feature that one can specify a range of eigenvalues to be computed, and thus avoid the computation of a complete eigensystem.

For the two and three-dimensional eigenproblems, we follow the general approach employed by Trellakis et.al. in [20] and use subspace iteration [16] with Chebyshev polynomial filtering. This procedure was developed because it targets the computation of the lowest states, is robust with respect to eigenvalue degeneracy, it can be made computationally efficient, and is relatively easy to implement. Other procedures [23,26] may prove more efficient, and these are under investigation.

The efficiency of the procedure used for the eigensystem computation, or for that matter, most iterative eigensystem routines, depends on the relative size of the spectral gaps between the eigenvalues and the spectral radius of the operator. In this particular problem there is the opportunity to reduce the spectral radius of the operator by projecting the eigensystem problem onto a lower dimensional subspace, a subspace that is rich enough in basis vectors to capture the eigenfunctions of interest (e.g. those associated with the lowest eigenvalues) and excludes those that lead to a large spectral radius but don't contribute to the wavefunctions of interest.

A reduced basis that leads to this reduction in spectral radius can be formed by changing the representation of the functions in the vertical direction from the standard grid node basis to one that consists of the lowest P eigenfunctions of the 1D Schroedinger operator in that direction. The idea here is to use vectors associated with vertical direction of the separable approximation (18) and (19) as the basis vectors for the non-separable approximation. As will be presented in the section on computational results, the number of vectors in the vertical direction that are required is quite small (approximately 10), and a dramatic improvement in computational performance can be obtained.

3.4. The Poisson equation

For layered domains, the separable nature of the Poisson problem allows one to create very efficient direct (e.g. non-iterative) Poisson solvers. The details of the solvers used are given in [1], however, for the readers convenience we summarize the main ideas behind them.

The potential in 1D satisfies a Poisson equation with piecewise constant, but discontinuous, coefficients (6). Moreover, the thin nature of the quantum wells demands that high resolution occur near the quantum wells. A method that has proven quite useful for such problems is an extension of a method by Wachspress [24]. Specifically, the solution is represented by a collection of locally exact solutions and the computational component consists of solving equations for the "free" constants in these solutions so that the local solutions join together to form a global solution. The benefit of this approach is that discontinuities and mesh refinement can be handled without difficulty as they occur at the junctions between the local solutions. The cost of obtaining this analytic solution is that of solving a symmetric, positive definite, tri-diagonal systems of equations, a task that can be accomplished in a computationally efficient manner (pivoting is not required). Moreover, because of the analytic nature of the solution, one can use extreme mesh coarsening in regions where the potential is not needed.

For problems in two and three dimensions one uses basis functions that are the product of one-dimensional basis functions in the vertical directions times Fourier modes in the transverse directions. For each Fourier mode in the transverse direction, the equation that describes its' variation in the vertical direction is a one-dimensional Helmholtz equation with discontinuous coefficients. Just as with the one dimensional Poisson problem, Wachpress's method can be extended to provide very accurate solutions of the one-dimensional Helmholtz equation for these Fourier coefficient. Since the transformation to the Fourier basis is accomplished using high quality FFT implementations (FFTW [7]), the procedure is computationally efficient.

The surface gates are represented by two-dimensional regions on the top of the device where a constant potential is specified. To avoid complications from discontinuities in the gate potentials, the values on the gates are extended smoothly to the free surface potential over a short distance away from the gate regions. This smoothing is necessary to avoid the oscillations in the computed potential due to Gibb's phenomenon.

A problem also arises in the computation of the potential when the doping for the devices is modeled as a sheet (e.g. two-dimensional) delta function. Rather than wrestle with the difficulties of representing sheet delta functions on a grid and then adding them to the other sources when solving the Poisson equation, the contribution to the potential due to these sources is computed analytically and added to the solution of the equation. In the case of doping with constant sheet density, the potential due to these sources is readily computed, as it is just a piecewise linear function whose coefficients are determined by requiring continuity of the potential and appropriate jumps in the derivatives at interfaces between layers of differing dielectric constants and at doping source locations. For variable sheet doping densities, one can compute a solution using techniques (and code) from the Fourier–Wachspress procedure [1].

3.5. Occupancy smoothing

The procedure we have described concerns the solution of the Schroedinger–Poisson equations in the zero-temperature limit, e.g. at 0 K. In this limit, the density of the 3D Schroedinger–Poisson equations (4) is discontinuous with respect to the occupied states. This discontinuity causes problems with convergence of the self-consistent iteration and to stabilize the iteration it is necessary to smooth this transition. We therefore use the formula for $n(x)$ that has the form,

$$n(\vec{x}) = 2 \sum_{E_k < E_F + \frac{\delta}{2}} \sigma_\delta(E_k) \Psi_k^*(\vec{x}) \Psi_k(\vec{x})$$

with $\sigma_\delta(E_k)$ is chosen to provide a smooth transition from 1 to 0 over the interval $\left[-\frac{\delta}{2}, \frac{\delta}{2}\right]$. The value of the smoothing parameter δ is chosen so that rapid convergence can be obtained and any further reduction in the smoothing parameter results in insignificant changes in the comptuational results. A typical transition width, δ, that is required to meet these two conditions is 0.0001 (e.g. in the units associated with the problem this corresponds to 0.1 milli-electron volts). For 1D and 2D, no smoothing is necessary. The discontinuity in the derivatives of the density with respect to occupied states (10) and (15) does not adversely effect the convergence since the iterative method is gradient free.

4. Computational results

To demonstrate results that can be obtained with the procedure described in the previous sections, we consider the simulation of a double well quantum device as depicted in Fig. 1.

This device has lateral dimensions 250 nm by 250 nm and a total height of 626.8 nm. The vertical structure consists of 6 layers, an AlInAs (20 nm) capping layer followed by InP (57.6 nm), InGaAs (12.6 nm), InP (10.6 nm), InGaAs (16 nm), and InP (510 nm). The device contains two delta doping layers with strengths $N_D = 3.5 \times 10^{11}$ cm^{-2} located at 40.5 nm and $N_D = 0.5 \times 10^{11}$ cm^{-2} located at 167.5 nm. The physcial parameters in Eqs. (1) and (2) were constant in each layer, and for AlInAs were $\kappa = 12.71, \beta = 0.073$ m$_0$, while for InGaAs they were $\kappa = 14.11, \beta = 0.043$ m$_0$ and for InP they were $\kappa = 12.61, \beta = 0.0795$ m$_0$. The band offset used for AlInAs was 0.252 eV and that used for InGaAs was -0.216 eV. The InP layers possesed a background doping density $\sigma_b = 3 \times 10^{15}$ cm^{-3}. All of the computations were done at 0 K.

In this device, the material properties of two thin layers of InGaAs induce potential wells that confine states in the vertical direction while voltages applied to the gates on the top of the device induce a potential that confines electrons in the transverse directions. In the upper well, it is desired to have isolated states forming "quantum dots" and in the lower well to have multiple states forming a "quantum wire".

Fig. 2(a) depicts the potential along a vertical centerline ($x = 0, y = 0, z \in [0, 400$ nm$]$) in the device and Fig. 2(b) depicts the transverse slice of the potential in the upper well (at $z = 84$ nm for $(x, y) \in [-250$ nm, -250 nm$] \times [250$ nm, 250 nm$]$). The square notches in the vertical potential are the quantum wells associated with the layers of InGaAs, and the kinks in the potential in the vertical direction are due to the discontinuous nature of the dielectric constants and the sheet doping. A notable feature of the potential in the transverse directions is the dip in the potential in the center; it is this dip in the potential that confines the states laterally in the upper well.

The operational nature of the device can be seen in Fig. 3 where the potential is rendered volumetrically with an isosurface of the charge density embedded within it. In Fig. 3(a) the gate bias is such that the charge density is confined to the

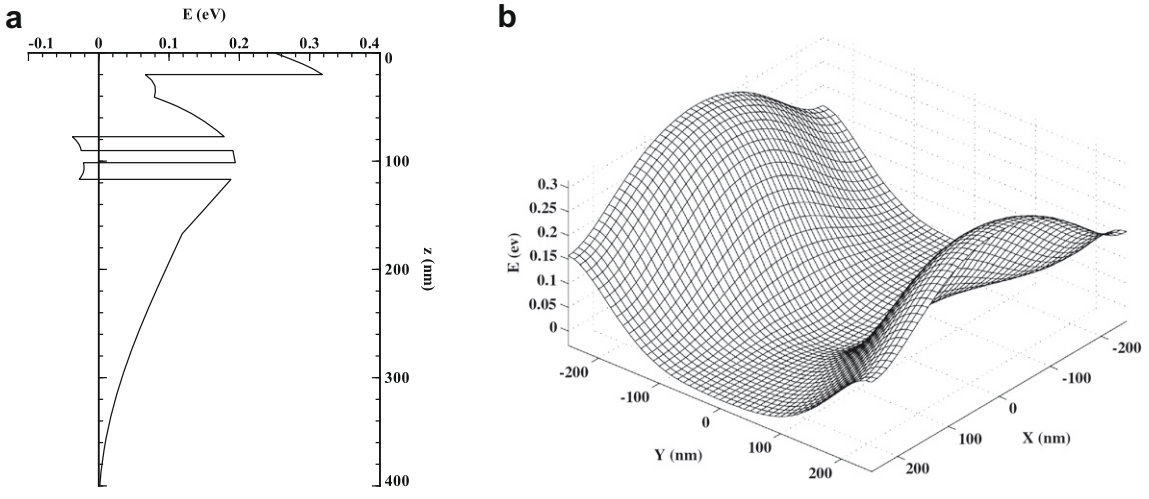

Fig. 2. (a) The potential along the vertical centerline and (b) the potential in the transverse directions in the center of the upper quantum well.

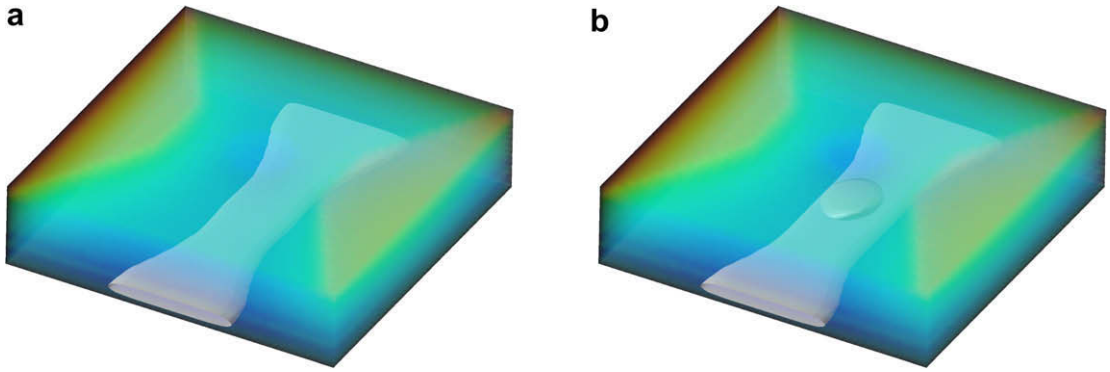

Fig. 3. Volumetric rendering of the potential with embedded isosufaces of the electron density for a double well quantum device. (a) Quantum wire in the lower well. (b) Quantum dot in upper well and quantum wire in lower well.

lower well, and forms a quantum wire that runs between the side gates. In Fig. 3(b), the potential on the center dot gate is lowered, and a single state occupies the lower well.

One of the principle reasons for simulating these devices is to be able to predict the occupancy of the upper quantum well as a function of the applied gate voltages. As occupancy occurs when the energy of the upper well states are below the fermi level, one needs to perform sweeps over applied gate voltages and monitor the energies associated with upper well states. If the original Schroedinger–Poisson equations (1) and (2) are used, then the computation of a single solution is very time consuming because of the need to compute the large number of the states associated with the quantum wire in the lower well. It is the need to carry out a large number simulations, and the substantial cost of each simulation that leads one to consider using the approximate models described in Section 2.

In Fig. 4(a) the energy of the lowest energy state in the upper well as a function of the gate voltage is presented. Two of the curves in Fig. 4(a) represent results obtained with models described in Section 2 and the third curve, that labelled "Quantum", represents results obtained by solving the original Schroedinger–Poisson equations (1) and (2). There are many combinations of the models that can be used to create approximate solutions, we are reporting those that have proven the most useful for design work (e.g. give the most satisfactory results with a minimum of computation time). In the use of these models the approximations are applied separately to the upper and lower well (e.g. a local computation). The need to use separate calculations is due to the fact that the approximation to the potential created for these models is more accurate when it is formed using values of the potential that are localized about each well. The first model utilizes the local density of states approximation (24) and (25) in both wells, the second uses a quantum-separable approximation (17)–(19) in both wells. In the full quantum simulation results, the energy is reported for gate voltages only when the upper well is non-empty, e.g. when among the lowest 10 energy states computed at least one of the states occupies the upper well. Energies for the other two models are reported for all gate voltages because they are results of a local (and hence separate) computation of the lowest energy states in the upper well.

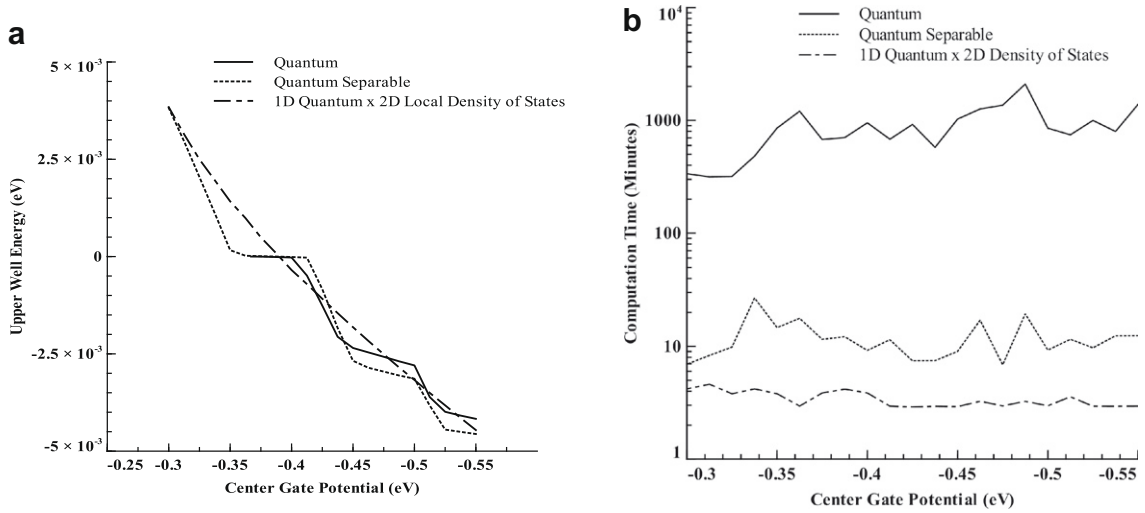

Fig. 4. (a) Energy of the lowest energy state in the upper well as a function of the gate voltage. (b) Computation times for results presented in (a).

Table 1
Computational results obtained with a reduced basis in the vertical direction and a standard nodal basis in the vertical direction.

Reduced basis size	Lowest eigenvalue	Spectral gap g_0	Spectral radius	Computational time (min.)
4	−0.01217886	0.005101	0.909	1.01
6	−0.01217918	0.004720	0.982	1.15
8	−0.01217957	0.004136	1.121	5.44
10	−0.01217969	0.003617	1.282	2.81
12	−0.01217972	0.003128	1.482	5.49
Standard basis	−0.01217974	0.000807	5.741	49.68

As is clear from a comparison of the results obtained with the models and that obtained by solving the original equations, the models do a good job of capturing the qualitative behavior of the device as the gate voltages are varied. Of course, the local density of states approximation does not explicitly utilize discrete states, so it is unable to capture the plateaus that occur when states are initially trapped in the upper well. However, the use of the quantum-separable model does capture this behavior rather well.

The computation times corresponding to the results in Fig. 4(a) are reported in Fig. 4(b). These results were obtained on machines equipped with an Intel Pentium IV processor, 3 GHZ clock speed, 2 GB of memory. The Linux operating system was used and the code was compiled using the GNU g++ compiler with -O2 optimization specified. For both the quantum-separable and fully quantum calculation, the results are those obtained when the local density of states approximation is used to provide an initial potential for the self-consistent iteration. These results demonstrate that solutions obtained with the approximate models can be obtained with a computation time that is more than an order of magnitude less than the solutions obtained by solving the original Schroedinger–Poisson equations.

As described in [1], for a fixed source distribution, the potential is approximately fourth order accurate. There is no loss in accuracy or smoothing associated with the discontinuous nature of the potential or its derivatives, as these features are handled explicitly in the solution procedure. The accuracy of the charge density and the energy values of the lowest energy states were observed to be at least second order accurate with respect to the mesh size. With a highly refined mesh in the vertical direction, the errors in the vertical direction are negligible, and the errors in the transverse direction dominate. In such cases, because of the high accuracy of the difference approximations in the transverse directions, the observed convergence rate was better than second order.

The last computational result we wish to present is the effectiveness of using a reduced basis for the solution of Schroedinger's equation. In this procedure, the standard nodal basis in the vertical direction is replaced by a basis consisting of a small number of the lowest states of the solution of the 1D Schroedinger equation in the vertical direction (e.g. solutions of (18)). In Table 1 the results of using a reduces basis with an increasing number of elements and with using the standard nodal basis is presented. Of particular interest in these results is the fact that with only 4 basis vectors in the vertical direction, the lowest eigenvalue is determined to four digits of accuracy; essentially the stopping tolerance used in the computation.

The computation times reported consist of that required for a single computation of the lowest 10 eigenstates. The dramatic reduction in the computation time that can be obtained when using the reduced basis is very clear. The method for computing the eigensystem is a variant of subspace iteration and its' efficiency is related to the time it takes to apply the Schroedinger operator to a given vector and the relative size of the spectral gap between eigenvalues, $g_k = \frac{|\lambda_k - \lambda_{k+1}|}{\max_j |\lambda_j|}$. Generally, the larger the gap size, the fewer iterations required to obtain convergence. One might think that the reduction of the computation time is due to fewer basis vectors being used in the vertical direction, and hence the application of the Schroedinger operator to a vector is reduced. This is not the case, since when using the reduced basis, the application of the operator is done in a nodal basis, and the work that is required is *more* per vector than with the nodal basis. The reduction in time is solely due to the change in the relative gap sizes. In Table 1 we give the relative size of the first gap, the other spectral gaps have similar behavior with respect to the size of the reduced basis set used. The reduction in gap size occurs because there is an increase in the spectral radius of the operator as the number of basis vectors is increased while the absolute gap size among the lowest eigenvalues is essentially unchanged.

5. Conclusions

In this paper we have presented approximations to the Schroedinger–Poisson equations that can be used to obtain qualitatively accurate, and often quantitatively accurate, results for the potential and states within layered semiconductor devices. These models can be used in a variety of ways; either directly to obtain approximate values for quantities of interest, or indirectly, with less accurate models providing initial iterates for the solution of more accurate models, or as a means of identifying basis functions that facilitate the rapid solution of Schroedingers equation.

Additionally, we have described a general algorithmic strategy that has proven successful as a means of solving the equations associated with each of these models. In any particular device simulation it is often difficult to tell in advance which approximate model will yield the best results, and one can only determine this by computational experiments. Having a single code that can compute solutions to all the different models is an asset when one when one is carrying out such experimentation.

In the Schroedinger–Poisson model spin effects are ignored. This is unfortunate, as it is the determination of the spin properties of the confined electrons that is of particular interest. However, once the device parameters have been identified that yield confined states, solutions of the Schroedinger–Poisson equations (or an approximation to them) still have value, as the Schroedinger–Poisson states can be used to provide candidate orbital basis sets for Hartree–Fock and Configuration–Interaction solution techniques that are required to solve an N-particle Schroedinger describing the confined states, e.g. in multi-resolution procedures similar to those described in [14,15].

Acknowledgments

This research was supported by DARPA through the Quantum Information Science and Technology (QuIST) program under Army Research Office contract number DAAD-19-01-C-0077. The author would like to thank Richard Ross and Mark Gyure for their invaluable advice during the development of the methods presented in this paper and the reviewers of this paper for their constructive comments. The author also appreciates the computational support provided by the National Science Foundation SCREMS grant #DMS-0112330.

References

[1] C.R. Anderson, T.C. Cecil, A Fourier–Wachspress method for solving Helmholtz's equation in three-dimensional layered domains, Journal of Computational Physics 205 (2) (2005) 706–718.
[2] C.R. Anderson, C. Elion, Accelerated solutions of nonlinear equations using stabilized Runge–Kutta methods, Tech. Rep. 04-26, UCLA CAM report, April 2004.
[3] E. Anderson, Z. Bai, C. Bischof, S. Blackford, J. Demmel, J. Dongarra, J. Du Croz, A. Greenbaum, S. Hammarling, A. McKenney, D. Sorensen, LAPACK Users' Guide, third ed., Society for Industrial and Applied Mathematics, Philadelphia, PA, 1999 (paperback).
[4] S. Bednarek, K. Lis, B. Szafran, Quantum dot defined in a two-dimensional electron gas at a n-AlGaAs/GaAs heterojunction: simulation of electrostatic potential and charging properties, Physical Review B (Condensed Matter and Materials Physics) 77 (11) (2008) 115320.
[5] S. Bednarek, B. Szafran, J. Adamowski, Theoretical description of electronic properties of vertical gated quantum dots, Physical Review B 64 (19) (2001) 195303.
[6] R.E. Caflisch, M.F. Gyure, H. Robinson, E. Yablonovitch, Modeling, design, and optimization of a solid state electron spin qubit, SIAM Journal on Applied Mathematics 65 (4) (2005) 1285–1304.
[7] M. Frigo, S. Johnson, The design and implementation of FFTW3, in: Proceedings of the IEEE 93, vol. 2, 2005, pp. 216–231, Special Issue on Program Generation, Optimization, and Platform Adaptation.
[8] R. Hanson, L.P. Kouwenhoven, J.R. Petta, S. Tarucha, L.M.K. Vandersypen, Spins in few-electron quantum dots, Reviews of Modern Physics 79 (4) (2007) 1217.
[9] M. Karner, A. Gehring, T. Grasser, H. Kosina, S. Selberherr, A multi-purpose Schroedinger–Poisson solver for TCAD applications, Journal of Computational Electronics 6 (1–3) (2007) 179–182.
[10] T. Kerkhoven, A. Galick, U.J.A. Ravaioli, Y. Saad, Efficient numerical simulation of electron states in quantum wires, Journal of Applied Physics 68 (7) (1990) 3461–3469.
[11] A. Kumar, S. Laux, F. Stern, Electron states in a GaAs quantum dot in a magnetic field, Physical Review B 42 (8) (1990) 5166–5175.
[12] S. Lapaul, A. de Lustrac, F. Bouillault, Solving the Poisson's and Schrodinger's equations to calculate the electron states in quantum nanostructures using the finite element method, IEEE Transactions on Magnetics 32 (3) (1996) 1018–1021.
[13] S. Laux, D. Frank, F. Stern, Quasi-one-dimensional electron states in a split-gate GaAs/AlGaAs heterostructure, Surface Science 196 (1–3) (1988) 101–106.
[14] D. Melnikov, P. Matagne, J. Leburton, D.G. Austing, G. Yu, S.J.F. Tarucha, N. Sobh, Spin configurations in circular and rectangular vertical quantum dots in a magnetic field: three-dimensional self-consistent simulations, Physical Review B (Condensed Matter and Materials Physics) 72 (8) (2005) 085331.
[15] D.V. Melnikov, J. Leburton, Dimensionality effects in the two-electron system in circular and elliptic quantum dots, Physical Review B (Condensed Matter and Materials Physics) 73 (8) (2006) 085320.
[16] B. Parlett, The Symmetric Eigenvalue Problem, SIAM, 1998.
[17] Silvaco, Atlas Device Simulation Framework, 2009. <http://www.silvaco.com>.
[18] J. Singh, Electronic and Optoelectronic Properties of Semiconductor Structures, Cambridge University Press, 2003.
[19] G. Snider, 1d Poisson/Schroedinger solver, 1996. <http://www.nd.edu/gsnider>.
[20] A. Trellakis, T. Andlauer, P. Vogl, Large-Scale Scientific Computing, Efficient Solution of the Schroedinger–Poisson Equations in Semiconductor Device Simulations, Springer, Berlin/Heidelberg, 2006.
[21] A. Trellakis, A.T. Galick, A. Pacelli, U. Ravaioli, Iteration scheme for the solution of the two-dimensional Schroedinger–Poisson equations in quantum structures, Journal of Applied Physics 81 (12) (1997) 7880–7884.
[22] A. Trellakis, T. Zibold, T. Andlauer, S. Birner, K. Smith, R. Morchl, P. Vogl, The 3d nanometer device project nextnano: concepts, methods, results, Journal of Computational Electronics 5 (4) (2006) 285–289.
[23] C. Vomel, S. Tomov, O. Marques, A. Canning, L. Wang, J. Dongarra, State-of-the-art eigensolvers for electronic structure calculations of large scale nanosystems, Journal of Computational Physics 227 (2008) 7113–7124.
[24] E. Wachspress, The numerical solution of boundary value problems, in: A. Ralston, H. Wilf (Eds.), Mathematical Methods for Digital Computers, John Wiley and Sons Inc., New York, 1964.
[25] L.-X. Zhang, P. Matagne, J.P. Leburton, R. Hanson, L.P. Kouwenhoven, Single-electron charging and detection in a laterally coupled quantum-dot circuit in the few-electron regime, Physical Review B 69 (24) (2004) 245301.
[26] Y. Zhou, Y. Saad, M. Tiago, J. Chelikowsky, Self-consistent-field calculations using Chebyshev-filtered subspace iteration, Journal of Computational Physics 219 (1) (2006) 172–184.